PROCEEDINGS OF SPIE

SPIEDigitalLibrary.org/conference-proceedings-of-spie

Organic thin film morphology, electronic structure, and effect on optoelectronic device

Wang, Shitan, Qian, Chuan, Huang, Han, Sun, Jia, Yang, Junliang, et al.

Shitan Wang, Chuan Qian, Han Huang, Jia Sun, Junliang Yang, Dongmei Niu, Haipeng Xie, Yongli Gao, "Organic thin film morphology, electronic structure, and effect on optoelectronic device," Proc. SPIE 11473, Organic and Hybrid Light Emitting Materials and Devices XXIV, 114730N (20 August 2020); doi: 10.1117/12.2572483



Event: SPIE Organic Photonics + Electronics, 2020, Online Only

Organic Thin Film Morphology, Electronic Structure, and Effect on Optoelectronic Device

Shitan Wang*a, Chuan Qian*b, Han Huanga, Jia Suna, Junliang Yanga, Dongmei Niua, Haipeng Xiea, Yongli Gaoc

^aHunan Key Laboratory for Super-Microstructure and Ultrafast Process, School of Physics and Electronics, Central South Univ., Changsha, Hunan 410012, People's Republic of China; ^bDept. of Chemical and Biomolecular Engineering, Yonsei Univ., Seoul 120-749, Republic of Korea; ^cDept. of Physics and Astronomy, Univ. of Rochester, Rochester, NY 14627, USA

ABSTRACT

There is a significant correlation in organic semiconductor thin films between the morphology and electronic structure, and both have strong effects on device performance. In this presentation, we describe our investigations on the relationship of the morphology and corresponding electronic structure and electrical properties using scanning probe microscopy techniques, photoemission spectroscopy, and transport measurements on organic semiconductor thin films. We also present investigations on the effects on optoelectronic device performance especially after controlling the morphology by quasi-epitaxial growth on representative organic semiconductors.

Keywords: Organic semiconductor, thin films, morphology, electronic structure, device performance, phototransistor

1. INTRODUCTION

Carrier mobility depends strongly on the morphology of organic semiconductors (OSC) that is used as the active layer in a device. 1-3 This is due to the very nature of the charge transport mechanism in OSC materials. In conventional inorganic semiconductors (ISCs), the atoms are held together firmly by strong covalent bonds, and charge carriers move as highly delocalized plane waves in wide bands. As a result, thermal fluctuations (phonons) will not disrupt long mean-free paths of charge carriers until relatively high temperatures are reached. Therefore, transport in ISCs is coherent, or band-like, which results in very high carrier mobilities. Unlike their inorganic counterparts, the OSCs have much weaker bonding forces (van der Waals forces) between their constituents.^{2, 4} Therefore, there will be a transition from band-like (which can be observed at low T) to incoherent hopping-type transport even at temperatures close to RT due to phonons. The mobility will increase with temperature but will have a limited value. In order to increase the temperature at which the transition from coherent to incoherent transport occurs, one needs to find -or synthesize- materials in which the intermolecular forces are much stronger. Materials such as members of the acene series, the most promising of which are pentacene and rubrene, have mobilities in the intermediate range between band transport and hopping (~10 cm²V⁻¹s⁻¹). The disparity between the best mobilities obtained in the OSCs and those obtained in ISCs is due to the dominance of incoherent hopping mechanism in the former case. Incoherent transport results from hopping between localized states, and charge carriers are scattered at every step. Due to this character of the transport in OSCs, the spatial order among different constituents is very important. Amorphous OSCs will, for instance, exhibit hopping-type transport at all temperatures. The morphology of the OSC films is therefore crucial to getting as high mobility as possible. Morphology has indeed been shown to be one of the main factors in deciding the final performance of an organic device. It has been demonstrated by many research groups that there is a strong correlation between the microstructure and the chargecarrier mobility in organic thin films. Charge carriers can hop easily from one molecule to another if there is ordering between them. However, lack of molecular ordering and presence of grain boundaries and impurities can be the greatest bottlenecks to charge transport in polycrystalline OSC thin films. Therefore, it is only natural to try to achieve quasiepitaxial growth with OSCs that will produce highly ordered films. After all, the success of today's silicon-based information technology hinges strongly on being able to fabricate epitaxial growth with ISCs.

There have been numerous attempts to improve the morphology of OSC thin films used in field-effect transistors (FETs). Jackson and co-workers have functionalized the active material (pentacene)/dielectric interface with a self-organizing material, octadecylthrichlorosilane (OTS), and obtained ordered morphology with larger single crystal domains. This, in turn, resulted in large carrier field-effect mobility, small sub-threshold slope and low threshold

Organic and Hybrid Light Emitting Materials and Devices XXIV, edited by Chihaya Adachi, Jang-Joo Kim, Franky So, Proc. of SPIE Vol. 11473, 114730N · © 2020 SPIE CCC code: 0277-786X/20/\$21 · doi: 10.1117/12.2572483

voltage.⁵ The OTS treatment is believed to improve the organic/dielectric interface.⁶ Shtein et al. observed that OTS treated interface resulted in higher crystallinity even though the final morphology was granular.⁷ This is likely due to the well-known though not well-understood fact that conductance is limited to the first few monolayers of the interface, where pentacene forms ordered thin films. Hence, the morphology of the higher monolayers is immaterial to the conductance. However, having many grain boundaries in the conducting channel of the organic thin film deteriorates the charge transport properties. In their work on the mobility dependence of polycrystalline oligothiophene thin films, Horowitz and Hajlaoui found that the mobility increases roughly linearly with grain size.⁸ Frisbie and co-workers measured on sexithiophene (6T) as high as $10^{10} \Omega$ resistance for a 1 μ m grain boundary length.⁹ That is why it is desirable to have highly ordered thin films in a device instead of polycrystalline ones with many grain boundaries. Sundar et al. achieved charge-carrier mobilities as high as $15 \text{ cm}^2\text{V}^{-1}\text{s}^{-1}$ by laminating a monolithic elastomeric stamp against the surface of a Rubrene crystal of the size of up to 3 mm.¹⁰

To understand the relationship between the morphology and electronic structure on device performance, we have studied the detailed evolution of morphology and electronic structure by means of ultraviolet photoemission spectroscopy (UPS), x-ray photoelectron spectroscopy (XPS), low energy electron diffraction (LEED), atomic force microscopy (AFM), Kalvin probe force microscopy (KPFM), current sensing AFM (CSAFM) and other supporting techniques. Growth on different substrates of copper phthalocyanine (CuPc) films, especially weak epitaxy growth (WEG) of CuPc with thin p-sexiphenyl (p-6P) template layer, were thoroughly investigated. High-performance organic heterojunction phototransistors based on WEG were fabricated with enhanced light absorption and photogenerated carriers. The results show intriguing relationships between the growth dynamics, electronic structure, device performance, and importance of grain boundaries and crystalline orientation.

2. RESULTS AND DISCUSSIONS

2.1 Molecular packing of CuPc on MoS₂ (0001)

CuPc is one of the most promising organic optoelectronic materials due to its advantageous attributes such as the excellent charge mobility and light absorption in visible range as well as the chemical and thermal stability. 11 To investigate the molecular packing of CuPc on MoS₂(0001), we implemented in situ LEED measurements. ¹² Fig. 1(a) shows the LEED pattern of clean MoS₂(0001). The sharp diffraction spots are in a hexagonal pattern, in accord with previous studies, ¹³ confirming its high quality. Fig. 1(b) shows the LEED pattern of 0.3 nm thick CuPc film with 12 broader diffraction spots in the inner circle, indicating that long-range ordered superstructures of CuPc with three equivalent domains 120° apart. 13 Fig. 1(c) and (d) illustrate the expected LEED pattern and molecular geometry of CuPc on MoS₂(0001). Fig. 1(e) shows the LEED pattern of 4.8 nm thick CuPc on MoS₂(0001) in a square symmetry, as indicated in Fig. 1(f) by the dashed white square grid, arising mainly from one out of the three domains in Fig. 1(d). This means that with the thickness increases from 0.3 to 4.8 nm, the average domain size may be enlarged, and the molecular plane remains (quasi-)parallel to the substrate. Otherwise, for CuPc in an edge-on configuration, the LEED pattern should be in a rectangular symmetry. It is in good agreement with previous studies of CuPc on layered substrates such as MoS₂, highly oriented pyrolytic graphite (HOPG), and graphene by theoretical calculations, ¹⁴ scanning tunneling microscopy (STM), 15 and noncontact AFM. 16 It should be noted that all of these studies were performed under ultra-high vacuum (UHV) conditions. Air exposure will turn CuPc on MoS₂(0001) edge-on, as demonstrated by x-ray diffraction (XRD) measurements. ¹² Additional support for the lying-down geometry of CuPc on MoS₂(0001) can be obtained from UPS as shown in Fig. 1(g), where the work function (WF) and ionization potential (IP) as a function of film thickness stay relatively constant to the values of lying-down ones, indicating the CuPc adopts lying-down geometry maintained in vacuum on MoS₂(0001).¹⁷ Presented in Fig. 1(h) is a representative zoomed-out AFM image (20 μm × 20 μm) to show the domain structure of 4.8 nm thick CuPc film. Overlaid at the bottom of the enlarged AFM image is the corresponding statistical distribution of the domain orientations relative to the horizontal direction. The zoom-in AFM image of a single domain is presented at the top right of Fig. 1(h), which shows that the domain is formed by highly aligned 1D nanocrystals. Statistically, the domain of aligned 1D nanocrystals have orientations relative to the horizontal direction (fast scanning direction of AFM) concentrated around $39 \pm 5^{\circ}$, $99 \pm 5^{\circ}$, and $159 \pm 5^{\circ}$, and the corresponding separation between them is $\sim 60^{\circ}$. 12

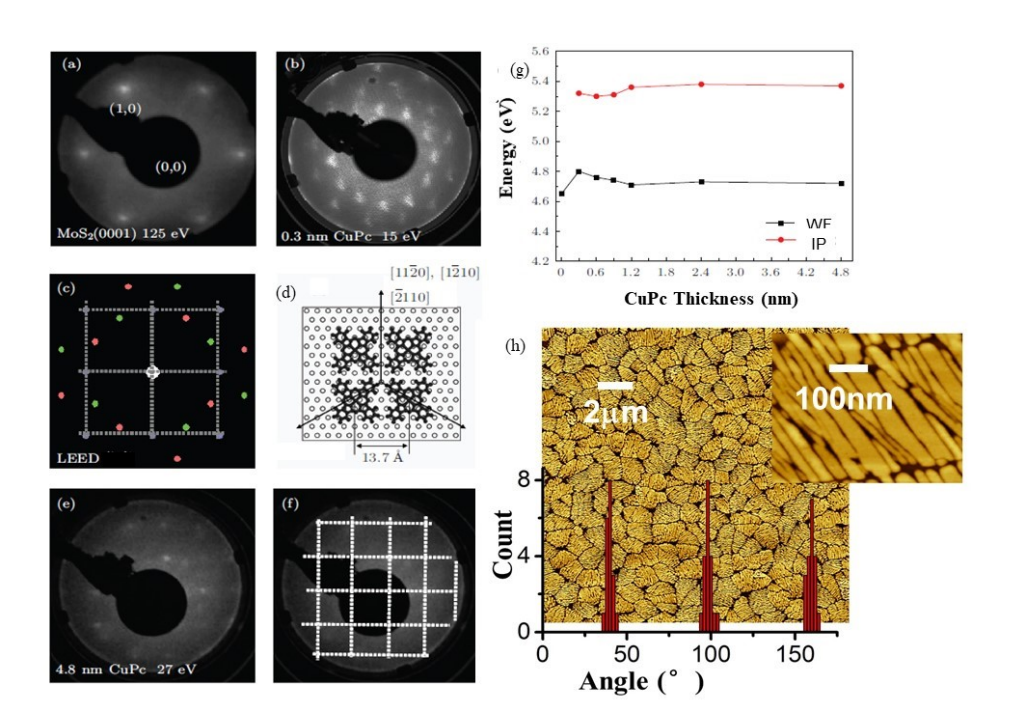


Figure 1. LEED patterns of (a) clean MoS₂ substrate and (b) 0.3 thick CuPc film on it at electron beam energies of 125 eV and 15 eV, respectively. (c) Expected LEED pattern and (d) molecular geometry of CuPc on MoS₂(0001). (c) LEED pattern of 4.8 nm thick CuPc film on MoS₂(0001) at electron beam energy of 27 eV. (f) LEED pattern of 4.8 nm thick CuPc film on MoS₂(0001) with a dashed square grid. A faint 4-fold symmetry can still be discerned. (g) Obtained from UPS, the work function and ionization potential of CuPc on MoS₂(0001) as a function of film thickness, indicating the CuPc adopts lying-down geometry when deposited and maintained in vacuum on MoS₂(0001). (h) AFM image (20 μm × 20 μm) of a 4.8 nm thick CuPc film. The corresponding statistical distribution of domain orientations relative to the horizontal AFM scan direction is overlaid at the bottom of the image. The zoom-in AFM image of a single domain is presented at the top right, which shows that the domain is formed by highly aligned 1D nanocrystals.

2.2 Islands reconstruction of CuPc on HOPG

We observed breaking down and reconstruction of islands in the film growth of CuPc on HOPG using UPS and AFM. At a critical thickness around 6 nm, the islands break down into small clusters. Further deposition drives the reunion of clusters to form large islands again and makes the film coverage smaller at a nominate thickness of 13 nm. The nonmonotonic photoemission spectroscopy (PES) data and AFM morphology confirmed the re-exposure of the substrate and the first layer CuPc during the island reconstruction process. ¹⁸ This nonmonotonic growth behavior may exist widely in many anisotropic molecular film growth processes where the thin film phases are confined or restricted by the symmetry of the substrate and different from their bulk phases.

Fig.2(a) shows the thickness θ dependence of the UPS on the CuPc/HOPG. The left panel shows the secondary electron cutoff region, the middle part shows the $Gr(\sigma^*)$ of HOPG, 19 and the right panel shows the highest occupied molecular orbital (HOMO) region. For the 0.3 nm and 0.6 nm CuPc films, the WF decreases by 0.07 eV relative to 4.6 eV of HOPG, indicating a weak dipole layer pointing from the CuPc side to the HOPG substrate. As θ increases from 0.6 nm to 4.8 nm, there is no apparent change in the WF. At the thickness of 7 nm, there is a sudden drop of the WF, and it reaches the minimum of 4.15 eV at θ = 9.0 nm. The decrease of WF indicates that the CuPc molecular orientation changes from lying-down to edge-on, which is consistent with previous studies by Ueno and Chen. Further deposition of CuPc to 11 nm and 13 nm shifts the WF upward by 0.1 eV and 0.21 eV, respectively, which is close to the WF of the stable bulk phase. The nonmonotonic variation, especially the drop of the WF, indicates that there are electronic and structural alternations with the transition from the substrate induced phase (SIP) to the bulk phase.

Shown in the middle of Fig. 2(a) is the intensity of the $Gr(\sigma^*)$ peak at 13.55 eV, originated from the conduction band of graphite. It also undergoes a nonmonotonic change with the deposition of CuPc from 0.3 nm to 13.0 nm. At $\theta < 9$ nm, the $Gr(\sigma^*)$ intensity keeps decreasing normally by the overlayer attenuation. Upon further deposition from 9 nm to 13 nm, instead of decreasing as ordinarily expected, the intensity of $Gr(\sigma^*)$ increases by about 10%. As shown in the right panel of Fig. 2(b), the HOMO consists of two components (the violet peak and orange peak) 0.17 eV apart. The fine structure of the HOMO peak has been attributed to the vibrational excitations of the hole in the CuPc thin film.36 For the 0.6 nm film, the HOMO peak shifts to the high BE side by about 0.06 eV and is located at BE = 1.24 eV with a full width at half maximum (FWHM) of 0.31 eV, while the vibration satellite can still be observed (the violet one). These changes in the position and width of the HOMO peak originate from the difference in the relaxation energies of the HOMO hole between the first (0.3 nm) and second (0.6 nm) CuPc layer. When θ reaches 2.4 nm, the HOMO region

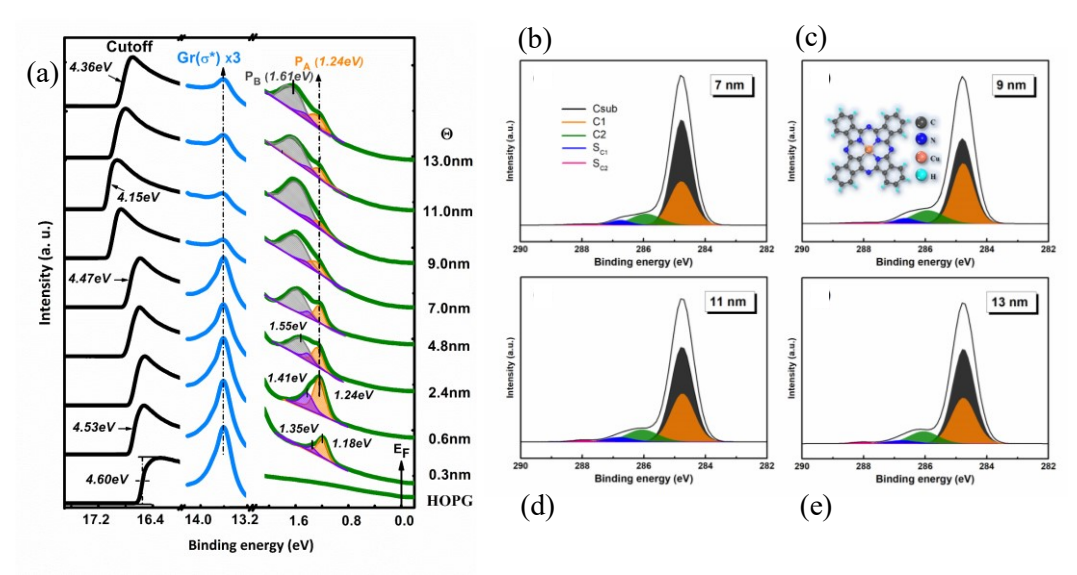


Figure 2. (a) UPS spectra of CuPc/HOPG with increasing CuPc film H (left) secondary electron cutoff region, (middle) $Gr(\sigma^*)$ peak from HOPG, and (right) the HOMO. (b) Film thickness dependence of the C1s core-level in CuPc on HOPG. C1s of 7 nm CuPc, and (c) 9 nm, (d) 11 nm, and (e) 13 nm CuPc film on HOPG. The C1s peak has been normalized before decomposing into four components: C_{sub} (black one), C2 (green one), C1 (orange one), S_{C1} (blue one), and S_{C2} (pink one). The inset of (b) shows the molecular structure of CuPc.

becomes broadened due to the appearance of a much stronger new component P_B centered at BE = 1.55 eV, which is from the π molecular orbital distributed over the inner porphyrin-like ring, ¹⁹ in addition to the interface P_A at 1.24 eV. As Ueno's group has previously pointed out, P_A is originated mainly from the interfacial thin film phase and P_B from the thick film phase of the CuPc domains. ²³ The evolution of the HOMO region reflects that a number of electrons from the thick film phase CuPc molecules (P_B) surpass that from the interfacial layers of CuPc molecules (P_A) with the deposition. The decrease in P_A before 9 nm is as expected because the interfacial layers of CuPc molecules are gradually covered by the thick film phase CuPc molecules. However, the abnormal increase in P_A at higher coverages ($\theta = 11$ and 13 nm) means that the interfacial layer of CuPc is re-exposed by a new phase transition process.

XPS provides further support on the phase transition process. Fig. 2(b)-(e) show the film thickness dependence of the C1s core-level. There is only one component of C 1s in HOPG (C_{sub}), which should be subjected to attenuation by the CuPc overlayer. There are four components of C 1s in CuPc, including that from the C-C bonds (C1 at 284.7 eV), the N-C=N bonds (C2 at 286.0 eV), and small satellites of C1 (S_{C1} at 286.7 eV) and C2 (S_{C2} at 288 eV).²⁴ With Gaussian-Lorentzian fitting and a fixed intensity ratio of (C1+ S_{C1}):(C2 + S_{C2}) = 1:3, the profiles are carefully decomposed, as shown in Fig. 2. The intensity of the C_{sub} peak from HOPG at θ = 7 nm decreases to a minimum at θ = 9.0 nm and then gradually increases as θ increases to 11nm and 13 nm. This increase runs parallel with the aforementioned abnormal increase in $Gr(\sigma^*)$ intensity from the substrate and from P_A at θ > 9 nm.

To highlight the correlations of the UPS, XPS and AFM results with the film growth, we summarize the energy levels and the schematic phase transition process in Fig. 3(a). At the interfacial layer, the adsorbate-substrate interaction is dominant, and so the CuPc molecules are bound to the substrate HOPG and grow into the interfacial layers with a stable lying-down configuration. There are three stages corresponding to the SIP, broken, and bulk phase building of the CuPc film after the interfacial layer. With the further deposition on the interfacial layer, the $\pi-\pi$ interaction of adsorbateadsorbate makes the deposited CuPc molecules maintain lying-down geometry and form some SIP islands. This first film growth stage is just as in the normal Stranski-Krastanov (S-K) mode in which signals from the HOPG decrease and the P_A of HOMO from interfacial layer CuPc molecules increases with the islands growth at $\theta < 7$ nm. This lying-down configuration of the SIP is an energetically metastable one, and further deposition leads to the accumulation of system energy until relaxation starts from the edge of the SIP islands and spreads throughout the whole film. Consequently, all the SIP islands break into clusters with higher coverage which induced the minimum photoelectrons from the substrates and the interfacial layer at 7 nm $< \theta < 9$ nm. With further relaxation and deposition, clusters aggregate and restack to form large bulk phase islands with standing-up orientation, leave deep grooves between neighboring islands, and make parts of the interfacial layer re-exposed. Therefore, the signals from the HOPG and interfacial layer of CuPc increase again. The change of molecular orientation was also confirmed using XRD.¹⁸ The proposed model shown at the bottom of Fig. 3(a) is consistent with the data presented in Fig. 3(b), where the valley shaped evolution of WF and the intensity of P_A , $Gr(\sigma^*)$ and C_{sub} peak are obvious with the CuPc deposition. In Fig. 3(b) the intensities of P_A , $Gr(\sigma^*)$ and C_{sub} peak have been normalized to the maximum of each.

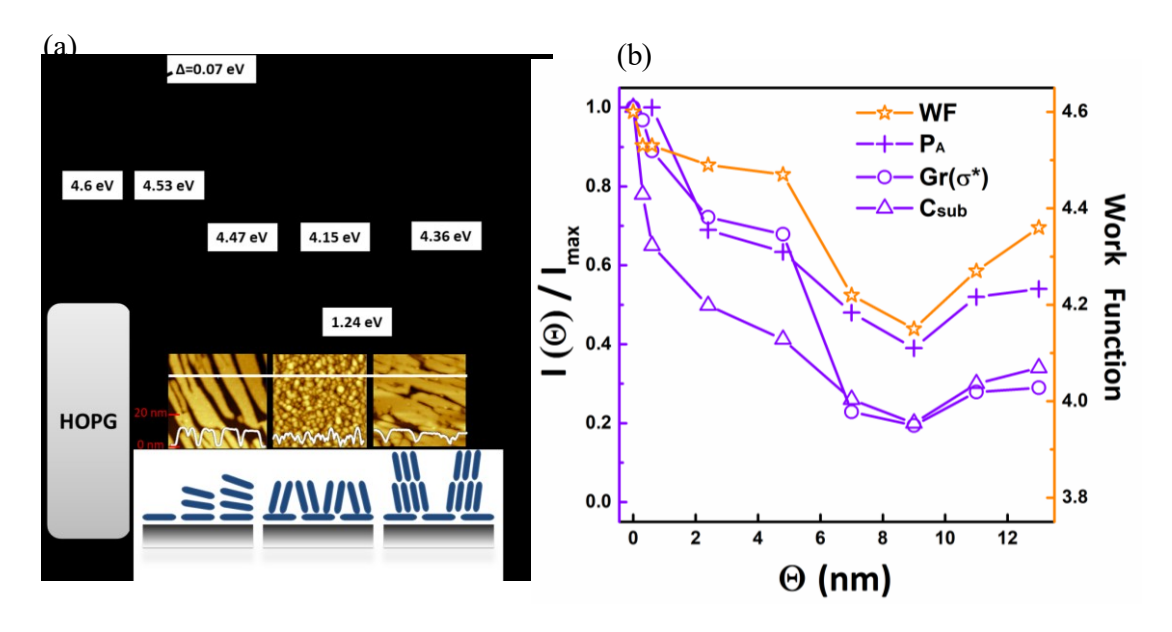


Figure 3. (a) The schematic drawing of energy level alignment for various thickness CuPc films on the HOPG substrate. AFM images (1 x 1 μ m) of 4.8 nm, 9 nm, and 13 nm CuPc films on HOPG in the middle and the cross sectional profiles corresponding to the white lines. The corresponding proposed molecular packing modes are shown at the bottom. (b) Valley shape evolution of WF and the intensity of P_A , $Gr(\sigma^*)$ and C_{sub} peak with the CuPc deposition, the intensities of P_A , $Gr(\sigma^*)$ and G_{sub} peak have been normalized to the maximum of each.

2.3 Weak epitaxy growth of CuPc on SiO₂

Conduction of electric charges is often done in polycrystalline organic thin films. Unavoidably, the crystallite size, orientation, and domain boundaries (DBs) affect the transport of the charge carriers. It is particularly so for organic semiconductors known to be highly anisotropic and strongly dependent on DBs. We have investigated the crystal-domain orientation and boundary on the charge transport in CuPc thin films quasi-epitaxially grown on p-sexiphenyl (*p*-6*P*) with Kelvin probe force microscopy.²⁵ In CuPc intra-domains, the voltage drop increases as the angle increases

between the domain orientation and the source-drain electric field. The increase of the DBs width and the angle between the orientations of neighboring domains results in the raise of voltage drop across the DBs, which restrict the charge transport in DBs simultaneously.

Weak epitaxy growth has been developed and succeeded in fabricating high-quality OSC thin films by introducing an ultrathin template molecular layer and elevating the growth temperature. The schematics of WEG is presented in Fig. 4(a). We grew WEG CuPc at a rate of about 1 nm/min recorded by a quartz crystal oscillator and at a substrate temperature of 180 °C on SiO₂ with p-6P template layers of various thicknesses. We fabricated organic FET configurations for KPFM measurements under operating conditions as shown in Fig. 4(b). The conductive tip of KPFM was also used in contact mode for CSAFM. Although CuPc thin films are usually polycrystalline with small grain sizes and many DBs that limit the performance of CuPc-based devices, WEG has been developed to fabricating high-quality CuPc thin films.²⁶ The sizes of CuPc crystalline domains can be dramatically increased to an average diameters of over 10 μm, leading to a significant improvement in carrier transport as demonstrated in FETs.²⁶ However, the microscopic picture and fundamental charge transport mechanism of these thin films were unclear. Given the present of intradomains and nanoscale DBs, the microstructure of CuPc thin films obtained by WEG is complicated. The noncontrollable domain orientations and boundaries may lead to large variations in the trap densities of the thin films

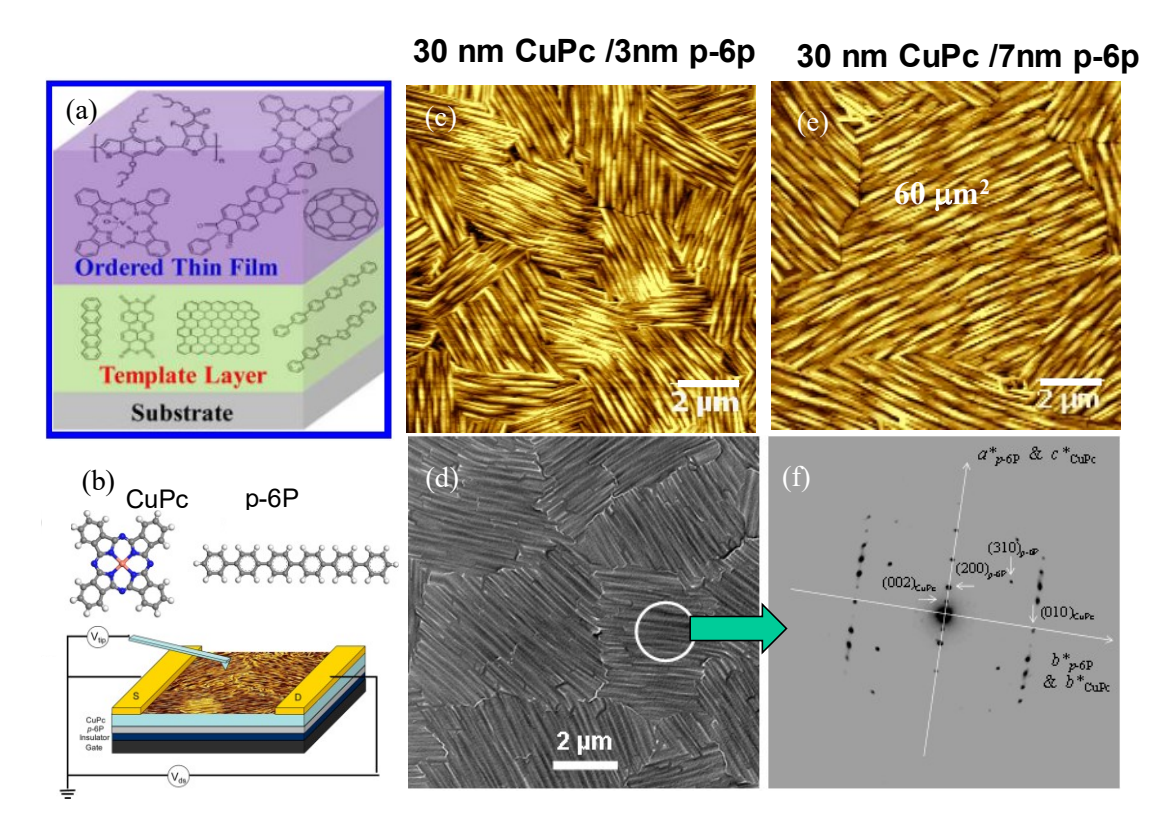


Figure 4. (a) Schematics of weak epitaxy growth. An ultrathin template molecular layer is inserted between the substrate and the active OSC, and the growth temperature is elevated. (b) Molecular structures of CuPc and p-6P. Field-effect transistor configuration is adopted for KPFM measurement under operating conditions. (c) AFM image ($10 \times 10 \, \mu m$) of 30 nm CuPc thin films grown on 3 nm p-6P template. (d) Transmission electron microscope (TEM) morphology of CuPc thin film grown on p-6P layer. (e) AFM image ($10 \times 10 \, \mu m$) of 30 nm CuPc thin films grown on 7 nm p-6P template. (f) SAED pattern of CuPc thin film grown on p-6P layer.

with different microstructures, resulting in nonuniform performances for those devices. Understanding their individual contributions to macroscopic charge transport at a microscopic level will enable us to assess the performance of the devices and help to optimize the microstructure of organic semiconductors with superior transport properties.

Kelvin probe force microscopy has been used as a powerful tool to study the morphological and electronic properties of thin films with nanoscale resolution by recording the electrostatic force interaction between the tip and the sample.²⁷ In

particular, KPFM can quantitative map the electronic properties of nanostructures and the potential of nano-objects. Fig. 4(c) and (e) show the morphologies of 30 nm CuPc thin films grown on p-6P layers of thicknesses of 3 nm and 7 nm, respectively. The CuPc molecules exhibit a stripe-like ordered structure in domains, formed by highly aligned 1D nanocrystals as the case of CuPc on MoS₂(0001) shown in Fig. 1. We adopt the term domain boundary to distinguish it from the boundary between the highly aligned 1D nanocrystals. The average domain size is about 10 μm² with 3 nm p-6P template layer (Fig. 4(c)), while it can be as large as 60 μm² with 7 nm p-6P (Fig. 4(d)). Shown in Fig. 4(d) is the transmission electron microscope (TEM) morphology of CuPc thin film grown on p-6P layer and in Fig. 4(f) its selected area electron diffraction (SAED) pattern. For the TEM measurements, CuPc/p-6P thin film was first deposited on SiO₂ substrate, and then a carbon film was deposited on CuPc/p-6P. The carbon film was used as the support layer. The thin film was separated from the SiO₂ surface by floatation in 10% HF solution and was transferred to a copper grid for the TEM measurement. The epitaxial relationship between CuPc and p-6P layer is clearly demonstrated and the corresponding orientations are (001)_{p-6P}//[100]_{CuPc}, [100]_{p-6P}//[001]_{CuPc}, [010]_{p-6P}//[010]_{CuPc}.

Shown in Fig. 5(a) is the AFM topographic image of Au electrodes and CuPc/p-6P channel with a single domain. The scan area is 5 μ m x 15 μ m. The topographic line scan of the dashed blue line in Fig. 5(a) is presented in Fig. 5(b). The flatness of the conducting channel and sharp steps at the Au electrodes are clearly illustrated. The thickness of the Au electrodes is about 45 nm and the length of the CuPc channel is about 12 μ m. Plotted in Fig. 5(c) are the typical I-V curves of Au-CuPc-Au of channel length 80 μ . with different sizes of domains of and 0, 20, and 70 μ m², respectively. CuPc grown directly on SiO₂ is taken to be the 0 μ m² one. It shows that the Au contacts are practically ohmic and the corresponding resistance is 9×10^9 Ω , 1×10^8 Ω , and 3×10^6 Ω , respectively. Clearly the resistance of the CuPc/p-6P thin film is greatly decreased with the domain size. Fig. 5(d) shows the field-effect mobility in CuPc FETs with different

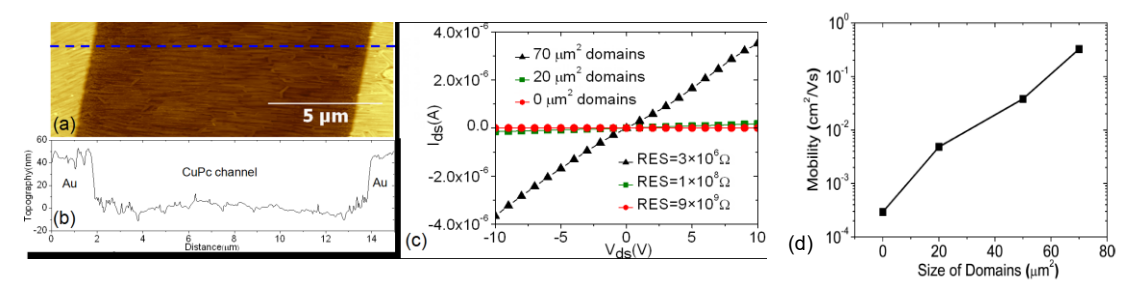


Figure 5. (a) is the AFM topographic image of Au electrodes and CuPc/p-6P channel with a single domain. The scan area is 5 μ m x 15 μ m. (b) The topographic line scan of the dashed blue line in (a). The flatness of the conducting channel and sharp steps at the Au electrodes are clearly illustrated. The thickness of the Au electrodes is about 45 nm and the length of the CuPc channel is about 12 μ m. (c) Typical I-V curves of Au-CuPc-Au of channel length 80 μ with different sizes of domains. (d) Field-effect mobility in CuPc OFETs with different sizes of domains in surface topography. The value of the size 0 is from CuPc thin film grown on bare SiO2 substrate with complete disorder. Note the mobility is semi-logarithmic to the domain area.

sizes of domains. This was investigated by depositing a series of thin films with increasing p-6P layer thickness and characterizing them with AFM. The mobility increases with domain size, in good agreement with published data. A hole field-effect mobility as high as $0.324~\rm cm^2V^{-1}s^{-1}$ was calculated in CuPc/p-6P thin film with the large oriented domain size of $70~\mu m^2$. The value is 3 orders of magnitude higher than OFETs with CuPc grown on bare SiO₂ substrate and is close to that of CuPc single crystals. The improved mobility is mainly due to the high quality of CuPc/p-6P film composed of large-area and oriented domains with fewer nanoscale boundaries. The increase of domain size can reduce the number of DBs, which results in the great decrease of the number of potential barriers for charge transport and weaken the misorientation degree and randomness of CuPc/p-6P film. Note that the mobility is semi-logarithmic to the average domain area instead of linearly with grain size.

Fig. 6(a) is the 4 μ m \times 10 μ m AFM topographic image of one Au electrode and adjacent CuPc domains. The topographic image shows that the DBs can be easily observed. The 1D crystallite orientations of the domains are marked by the purple arrows. The corresponding KPFM potential image is plotted in Fig. 6(b). It can be seen that while the Au electrode protrudes strongly in the AFM image, its voltage is low and constant. While the domain wall in the AFM topographic image is overshadowed by the Au electrode, the potential image clearly shows that there is a voltage drop across the DB. The topographic line scan of the dashed blue line in Fig. 6(a) is presented in Fig. 6(c) and the potential

line scan of the dashed blue line in Fig. 6(b) is presented in Fig. 6(d). In the topographic line scan, the DB is seen as an apparent dip of 20 nm. The true shape of the dip is hard to image as the tip contour has to be convoluted into the scan. The potential line scan presents a steep drop of 335 mV across the DB, indicating that a single DB can contribute almost 7% drop out of the total bias of 5 V between the two Au electrodes. More close inspection reveals that the slope of intra-domain potential drop depends on the 1D crystallite orientation, and it is smaller if the orientation is more aligned with the direction of the current. It makes sense as the charge carriers should transport more easily along the crystallites than hopping across adjacent ones.

The topographic and potential line scans parallel to each other and ~1 µm apart across the same DB are shown in Fig. 7(a) and (b), respectively. The topographic line profile 3 shows a DB width of about 89 nm, and the corresponding voltage drop is about 120.4 mV, in which the potential drops abruptly. It obviously suggests that the abrupt potential steps are present in the voltage drop images caused by the DBs in the film, which results from a structural discontinuity

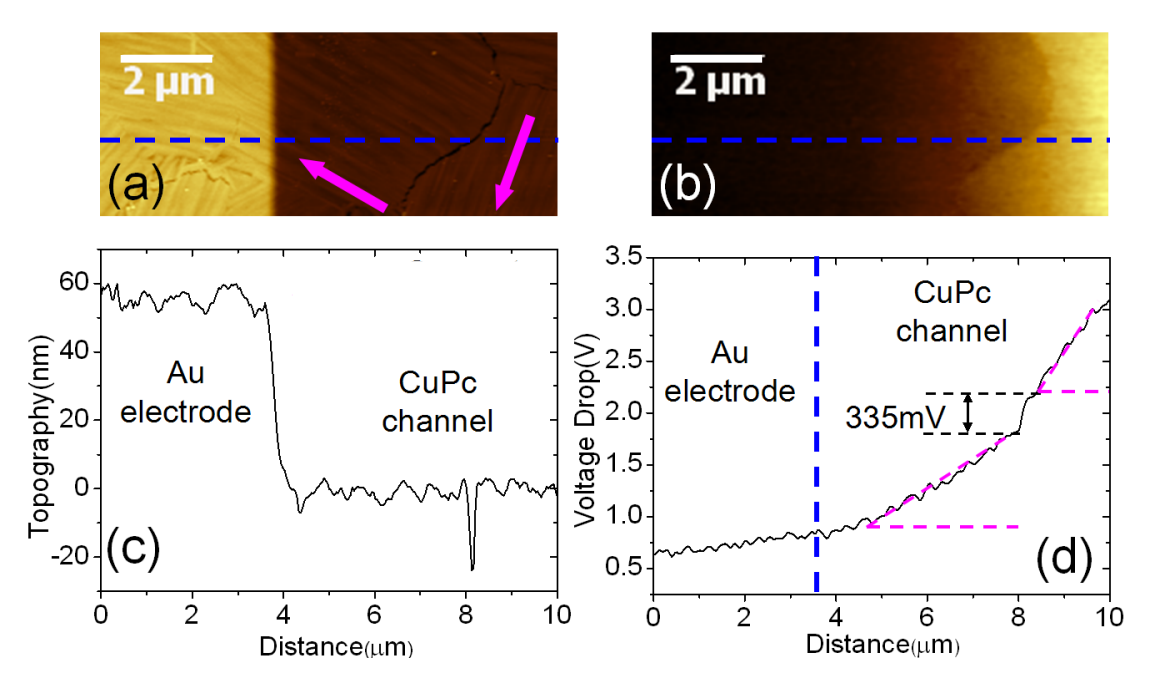


Figure 6. (a) 4 μ m ×10 μ m AFM topographic image of one Au electrode and adjacent CuPc domains. The DB can be easily observed. The 1D crystallite orientations of the domains are marked by the purple arrows. (b) KPFM potential image corresponding to the topography in (a). The potential image shows a voltage drop across the DB. (c) The topographic line scan of the dashed blue line in (a). The DB is seen as an apparent dip of 20 nm. (d) The potential line scan of the dashed blue line in (b). There is a steep potential drop of 335 mV across the DB. The slope of intra-domain potential drop is smaller if the orientation is more aligned with the direction of the current.

in the molecular packing. Line profile 4 indicates that the width of DB is about 60 nm and the corresponding voltage drop is 99.8 mV. Line profile 5 shows that the width of DB is about 32 nm, which is the narrowest width at the DBs and results in the smallest voltage drop of 66.6 mV. In other words, the voltage drop becomes higher with the width of the DBs increased. As far as the depth of DBs is concerned, the scanning signal of topography has a little distortion at DBs based on AFM mechanism. Because the CuPc with a thickness of 30 nm was epitaxially grown on the surface of second layer p-6P thin film with disconnected islands, the DBs of a CuPc film are formed. So, the depth of DBs is about 30 nm.

Fig. 7(c) provides a statistic characterization of the width of the associated potential drop per micron, and the values of the voltage drop rate change a little with the width of DBs ranging from 50 to 105 nm. All data are obtained from the angle range of $75 \pm 5^{\circ}$ between the orientations of two connected domains. Each point is the average of the five or more scans, and the standard deviation is also plotted. The voltage drop increases with the width of the DB. It confirms that the charge carriers are easy to go through a lower back-to-back Schottky barrier at the DBs with a narrower width by thermionic emission. By reducing the width of DBs, the effect of the DBs on the charge transport would be reduced, and

the voltage drop is decreased accordingly. The nanoscale DBs system can be very complicated.35,36 However, we do observe that the voltage drop rate across the DB is practically independent on the DB width, as the data in Figure 7(c) indicate. It suggests that the charge transport across a DB is by diffusion instead of by tunneling or variable range hopping.²⁹ It remains to be explored if this effect depends on the p-6P template layer.

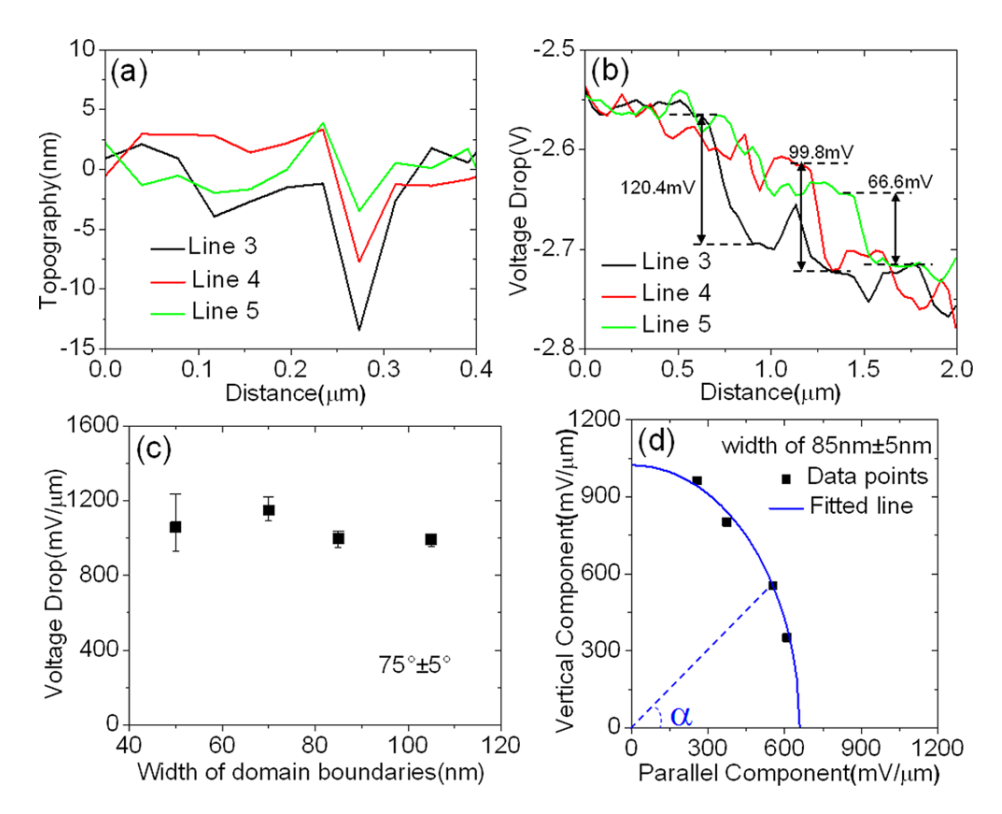


Figure 7. (a) Parallel topographic line scans 1 μ m apart across the same GB. The widths of the GBs are 89, 60, and 32 nm, respectively. (b) The corresponding line cross sections of voltage drop at each GB, which are 120.4, 99.8, and 66.6 mV, respectively. (c) Scatter diagram for the correlation between the voltage drop per micron and the width of the domain boundaries. Each point is the average of the five or more scans. All data within the angle of the orientation of two connected domains for the angle range of $75 \pm 5^{\circ}$. (d) The correlation between the voltage drop per micron and the angle of the orientation of two connected domains. Each point is the average of the five or more data. All data within the width of domain boundaries for the range of 85 ± 5 nm. The blue line shows the elliptical orientational fitted transformation of the voltage drop tensor. The maximum and minimum voltage drop values occur along the vertical direction (90°) and parallel direction (0°), respectively.

Fig. 7(d) presents a statistic characterization of the misorientation angle α between two adjacent domains and the associated potential drop rate. All data are obtained from DBs with width of 85 ± 5 nm. Each point is the average of five or more measurements, and the standard deviation is smaller than or equal to $80 \text{ mV/}\mu\text{m}$. It can be seen that the voltage drop increases with α . Chwang and Frisbie found that as the angle of misorientation between the two grains increases, the carriers are harder to across the grain boundary. It is interesting to explore the possible reasons about the increase of the misorientation angle α between the orientations of two connected domains restrict the transport of charge carriers in the DBs. The domains can be assumed as big CuPc "molecules" which are standing-up arrangement on the substrate. The π -electron clouds of the neighboring "molecules" begin to overlap with the angle α decreasing from 90° to 0° . The overlap of electron clouds is convenient for the carriers transport. Another possible reason is related to the charge scattering. The carriers cross a back-to-back Schottky barrier at the interface between two CuPc domains with different orientations, and electron scattering will occur at the interface. The increase of domain misorientation results in a large probability of electronic scattering and the mean free path becomes short, which leads to a large voltage drop. Just like phase transition at the interface, the more the inter-domain angle α increases, the greater the electron scattering. As the

organic semiconductor is anis again assumed elliptical anisotropy for the orientational dependence. In Fig. 7(d), we have fitted the voltage drop ΔV by the elliptical orientational dependence of the α as:

$$\Delta V = \frac{AL_D}{\sqrt{1 + B\cos\alpha}}$$

where L_D is the domain size, and A and B are fitting parameters denoting the magnitude and ellipticity of the voltage drop. We deduced fitting parameters for the magnitude $A = 1024 \text{ mV/}\mu\text{m}^2$ and ellipticity B = 1.41. The long and short axis thus obtained are 2047 mV/ μ m and 1318 mV/ μ m, respectively. From the fitting line shown in Fig. 7(d) it looks that the elliptical anisotropy is a reasonable fit.

2.4 Organic heterojunction phototransistors with WEG CuPc

We have fabricated high-performance organic heterojunction phototransistors with enhanced light absorption and photogenerated carriers using WEG CuPc. Under 365 nm ultraviolet light irradiation, the ratio of photocurrent and dark current and photoresponsivity of CuPc/p-6P heterojunction phototransistors reaches to about 2.2×10⁴ and 4.3×10² A/W, respectively, about two orders of magnitude improvement on those without the p-6P underlining.³¹

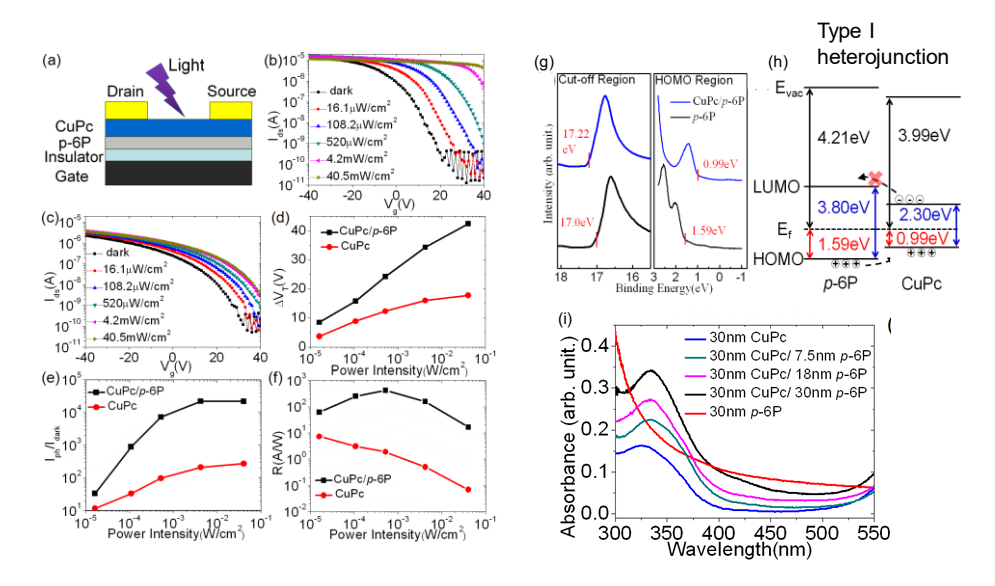


Figure 8. (a) Structure schematic of CuPc/p-6P heterojunction phototransistors. The typical transfer characteristics of (b) CuPc/p-6P and (c) CuPc phototransistors, respectively, measured in the dark or under UV (365 nm) with various light intensities at $V_{ds} = -50$ V. (d) The ΔV_T of CuPc/p-6P and CuPc phototransistors as a function of power intensity. (e) The I_{ph}/I_{dark} of CuPc/p-6P and CuPc phototransistors as a function of power intensity at V_{on} . (f) The photoresponsivity of CuPc/p-6P and CuPc phototransistors as a function of power intensity at V_{on} . (g) UPS spectra for p-6P and CuPc/p-6P. (h) The interface energy level alignment can be determined to be type I heterojunction with HOMO offset of 0.60 eV. (i) UV–vis absorption spectra of CuPc, CuPc/p-6P, and p-6P thin films on glass substrate.

Based on disordered CuPc and highly ordered CuPc/p-6P thin films, the corresponding phototransistors were fabricated, and the structure schematic of CuPc/p-6P heterojunction phototransistors is shown in Fig. 8(a). The typical transfer characteristics of CuPc/p-6P and CuPc phototransistors are shown in Fig. 8(b) and (c), which were measured in the dark or under UV (365 nm) with various light intensities at $V_{ds} = -50$ V. The mobility of CuPc/p-6P thin films have been reported that a hole field-effect mobility as high as 0.18 cm²V⁻¹s⁻¹ could be obtained, which was about 2 orders of magnitude higher than that of CuPc based field-effect transistors (FETs) ($\approx 2.1 \times 10^{-3}$ cm²V⁻¹s⁻¹).²⁵ The results in Fig. 8(b) and (c) show that, under the dark condition, the off-current of CuPc/p-6P and CuPc phototransistors is about 1.6 × 10^{-11} and 1.2×10^{-11} A, respectively, while the on-current of two devices is about 1.4×10^{-5} and 1.2×10^{-6} A,

respectively. Because the highly ordered CuPc thin films with large-size grain can greatly improve the charge transport, and the electrical properties of CuPc/p-6P phototransistors are much better than that of CuPc FETs.

For both CuPc/p-6P and CuPc phototransistors, the I_{ds} measured under UV irradiation show an obvious threshold voltage (V_T) shift, indicating that light acts as an additional control terminal to photogenerated carriers. Theoretically speaking, the photon would be absorbed, and a number of charge carriers can be photogenerated as the photon energy is equal to or higher than the band-gap energy of semiconductor thin films. The results in Fig. 8(b) and (c) suggest that, under the UV light, there is only a small current change in CuPc phototransistors while a very large current change can be observed in CuPc/p-6P heterojunction phototransistors. The typical transfer curves for these phototransistors show the obvious current change. Furthermore, there is an obvious positive shift in V_T with increasing power intensity. The V_T of CuPc/p-6P and CuPc phototransistors in the dark are about 9.0 and 20 V, respectively. When the devices are irradiated with 40.5 mW cm⁻² UV light, the V_T of CuPc/p-6P phototransistors positively shift to be about 51.4 V and the difference between the V_T (Δ V_T) is 42.4 V. For CuPc phototransistors, the V_T positively shift to be 37.8 V and the Δ V_T is 17.8 V, which are much smaller than that of CuPc/p-6P heterojunction phototransistors.

The ΔV_T of CuPc/p-6P and CuPc phototransistors under light as a function of power intensity is shown in Fig. 8(d). The logarithm of ΔV_T shows a linear relationship with the light power intensity, known to reflect the number of trap charges.³² In our devices, a larger ΔV_T was observed in CuPc/p-6P phototransistors. Thus, more photogenerated electrons may be trapped at the CuPc/p-6P interface, which provides a larger response window to different light densities and the recombination rate might be reduced accordingly.

For phototransistors, both light and gate electrode are useful to control the carriers in the channel. The I_{ph}/I_{dark} is an important parameter to evaluate the performance of phototransistors. As shown in Fig. 8(e), the I_{ph}/I_{dark} was obtained at $V_{on}=20~V$ of CuPc/p-6P devices. At turn-on voltage, the increased holes are mainly photogenerated and are not the effect of electrically induced hole by the gate electrode. Specifically, the I_{ph}/I_{dark} dramatically increases with increasing the incident light power, and it would not obviously change any more when the light power is above 4.0 mW cm⁻². The maximum I_{ph}/I_{dark} is 2.2×10^4 under $4.2~mW~cm^{-2}$ UV light and the photogenerated carriers become saturated in the channel. Under the same condition, the maximum I_{ph}/I_{dark} of CuPc phototransistors is 2.7×10^2 at $V_{on}=32~V$, which is almost two orders of magnitude smaller than that of CuPc/p-6P one. Another important parameter is photoresponsivity (R), which indicates the capability of photoelectric conversion and is defined as the ratio of the photocurrent to the incident optical power on the active area of phototransistors. As shown in Fig. 8(f), the maximum photoresponsivity of CuPc/p-6P heterojunction phototransistors is about 59 times larger than that of the CuPc device

The UPS spectra for p-6P and CuPc/p-6P are shown in Fig. 8(g). From the measured HOMO and vacuum level cutoff the interface energy level alignment can be determined to be type I heterojunction with HOMO offset of 0.60 eV, as illustrated in Fig. 8(h). As shown in Fig. 8(i), the p-6P thin film has strong absorption in the UV region; thus, a lot of holes and electrons are probably photogenerated in each separated island. For CuPc/p-6P phototransistors, the CuPc/p-6P heterojunction interface acts as an effective charge transport channel.

We have applied CSAFM on CuPc and CuPc/p-6P phototransistors to obtain quantitative information of spatial variations about the size, shape, and distribution of conducting nanostructure in the modified morphology with nanoscale resolution. The topographic images of highly oriented CuPc/p-6P thin film and disordered CuPc thin film are shown in Fig. 9(a) and (b), respectively. The DBs between two highly oriented grains can be easily observed in the CuPc/p-6P thin film. The corresponding surface conductivity image of CuPc/p-6P thin film under dark is shown in Fig. 9(c). The current image shows the same track to its topography. The values of current imaged by CSAFM in contact-mode are displayed from the black (the highest absolute value) to the white (the lowest absolute value). In the polycrystalline thin film, the model of charge transport includes a high conductivity region and low conductivity region. There is a remarkable difference between the intra-domains and DBs. At the DBs, the absolute current is obviously about 8 pA smaller than the value at intra-domain. More conductive region evidently exists in domains, because the intra-domains have single-crystal-like properties and the traps are located in the DBs. The corresponding surface conductivities image of CuPc thin film under dark is shown in Fig. 9(d), which demonstrates a lower absolute current on the thin film surface. There are a large number of DBs in the thin film. The absolute current is higher in the

grains than that at the DBs. The carriertransport process is more effective on the grains. Compared to the current image of CuPc/p-6P thin film in Fig. 9(c), the conductive region of CuPc thin film is much smaller. For the CSAFM measurement, a weak power density of 365 nm light was used to irradiate the sample. It is able to control the conductance by absorption of light. As shown in Fig. 9(e), the absolute current in grain increases and the current at the DBs show little change under light. The DBs between domains in CuPc/p-6P thin film are existing in discontinuous areas between p-6P islands. Without the CuPc/p-6P heterojunction, the DBs would photo generate less holes and these holes are easy to be trapped by existed traps in the DBs. It is clear that the photocurrent is not averagely distributed over the whole surface of the thin film but mainly generated in the region of ordered domains with CuPc/p-6P heterojunction. The photocurrent in the CuPc/p-6P thin film is much bigger than that in the CuPc thin film because of the highly ordered thin film structure. There is almost no photocurrent observed in the CuPc thin film. The absolute currents generated by the UV light in CuPc/p-6P and CuPc thin films are about 5.5 and 1 pA, respectively, as shown in Fig. 9(f).

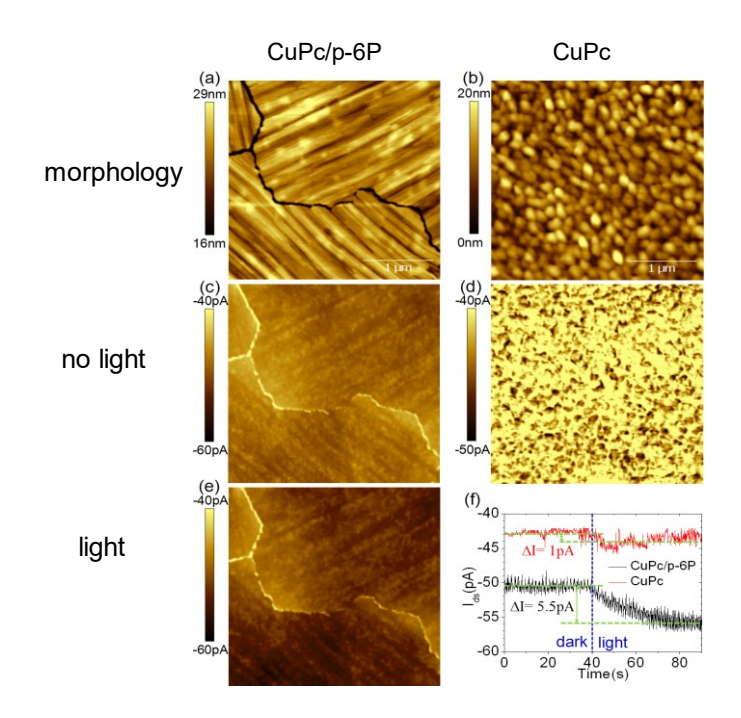


Figure 9. Topographic images of (a) CuPc/p-6P thin film and (b) CuPc thin film. The corresponding current images of (c) CuPc/p-6P thin film under dark, (d) CuPc thin film under dark and (e) CuPc/p-6P thin film under light. The scan area is 3 μ m \times 3 μ m. (f) The change of current detected by the tip asfunction of time under dark (time < 40 s) or under light (time \geq 40 s).

3. CONCLUSIONS

We presented our investigations on the correlation between the morphology and electronic structure and the effects on device performance. we have studied the growth and modifications of CuPc on different substrates and in the weak epitaxial growth mode. We found that CuPc forms well-ordered 1D nanocrystals on layered substrates MoS₂ and HOPG, and changing from the substrate induced phase to the bulk phase can be accompanied by re-exposure of the interface. WEG growth of CuPc on p-6P template can produce high quality thin films with domains of with apparently highly aligned 1D nanocrystals, and the domain size can be controlled by the thickness of the template layer. The mobility of CuPc/p-6P increases semi-logarithmically to the domain area. The voltage drop across the domain walls is influenced by the width of DBs and the angle of the 1D nanocrystal alignment in the neighboring domains. The voltage drop rate in terms of volt per micron across the DB is practically independent on the DB width, suggesting that the charge transport across a DB is by diffusion instead of by tunneling or variable range hopping. The angular dependence of the charge transport is found to be elliptical on the relative orientation of the neighboring domains. Highperformance organic heterojunction phototransistors based on WEG CuPc/p-6P were demonstrated and characterized, with performance much superior than that without the molecular template. Detailed analysis reveals that DBs are inactive in generating photocurrent, and the performance enhancement is achieved by diminishing the inactivity of DBs and enhancing charge transport mobility. The results show that understanding the growth dynamics and morphology and introducing means to control them are essential and fundamental to performance enhancement in organic optoelectronic devices.

ACKNOWLEDGMENTS

This work is supported in part by the National Natural Science Foundation of China (Grant Nos. 11334014, 51802355, 61975241, 51673214). H.X. acknowledges the support by the Natural Science Foundation of Hunan Province (Grant No. 2018JJ3625). Y. G. acknowledges the support from National Science Foundation DMR-1903962.

REFERENCES

- * These authors contribute equally to the article.
- 1. Horowitz, G., "Organic Field-Effect Transistors" Adv. Mater. 10, 365 (1998).
- 2. Bolognesi, A., Di Carlo, A., Lugli, P., Conte, G., "Large drift-diffusion and Monte Carlo modeling of organic semiconductor devices," Synthetic Metals 138 (1-2), 95-100 (2003).
- 3. Ma, W. L., Yang, C. Y., Gong, X., Lee, K., Heeger, A. J., "Thermally stable, efficient polymer solar cells with nanoscale control of the interpenetrating network morphology," Advanced Functional Materials 15 (10), 1617-1622 (2005).
- 4. Schroeder, P. G., France, C. B., Park, J. B., Parkinson, B. A., "Orbital alignment and morphology of pentacene deposited on Au(111) and SnS2 studied using photoemission spectroscopy," Journal of Physical Chemistry B 107 (10), 2253-2261 (2003).
- 5. Nelson, S. F., Lin, Y.-Y., Gundlach, D. J., Jackson, T. N., "Temperature-independent transport in high-mobility pentacene transistors," Applied Physics Letters 72, 1854-1856 (1998).
- 6. Dimitrakopoulos, C. D., Malenfant, P. R. L., "Organic Thin Film Transistors for Large Area Electronics " Adv. Mater. 14, 99-117 (2002).
- 7. Shtein, M., Mapel, J., Benziger, J. B., Forrest, S. R., "Effects of film morphology and gate dielectric surface preparation on the electrical characteristics of organic-vapor-phase-deposited pentacene thin-film transistors "Appl. Phys. Lett. 81, 268-270 (2002).
- 8. Horowitz, G., Hajlaoui, M. E., "Mobility in Polycrystalline Oligothiophene Field Effect Transistors Dependent on Grain Size," Adv. Mater. 12, 1046-1050 (2000).
- 9. Loiacono, M. J., Granstrom, E. L., Frisbie, C. D., "Investigation of Charge Transport in Thin, Doped Sexithiophene Crystals by Conducting Probe Atomic Force Microscopy," J. Phys. Chem. B 102, 1679–1688 (1998).
- Sundar, V. C., Zaumseil, J., Podzorov, V., Menard, E., Willett, R. L., Someya, T., Gershenson, M. E., Rogers, J. A., "Elastomeric transistor stamps: reversible probing of charge transport in organic crystals " Science 303, 1644-1646 (2004).
- 11. Chen, S., Ma, J., "The Influence of Orientations and External Electric Field on Charge Carrier Mobilities in CuPc and F16CuPc Films on Highly Ordered Pyrolytic Graphite and Octane-1-Thiol Terminated Au(111) Substrates," Phys. Chem. Chem. Phys. 12, 12177–12187. (2010).
- 12. Zhang, L., Yang, Y., Huang, H., Lyu, L., Zhang, H., Cao, N., Xie, H., Gao, X., Niu, D., Gao, Y., "Thickness-Dependent Air-Exposure-Induced Phase Transition of CuPc Ultrathin Films to Well-Ordered One-Dimensional Nanocrystals on Layered Substrates," Journal of Physical Chemistry C 119 (8), 4217-4223 (2015).
- 13. Collins, G. E., Nebesny, K. W., England, C. D., Chau, L. K., Lee, P. A., Parkinson, B. A., Armstrong, N. R., "Orientation and Structure of Monolayer→Multilayer Phthalocyanine Thin Films on Layered Semiconductor (MoS2 and SnS2) Surfaces. ," J. Vac. Sci. Technol. A 10, 2902–2912. (1992).
- 14. Xiao, K., Deng, W., Keum, J. K., Yoon, K., Vlassiouk, I. V., Clark, K. W., Li, A. P., Kravchenko, I. I., Gu, G., Payzant, E. A., Sumpter, B. G., Smith, S. C., Browning, J. F., Geohegan, D. B., "Surface-Induced Orientation Control of CuPc Molecules for the Epitaxial Growth of Highly Ordered Organic Crystals on Graphene," J. Am. Chem. Soc. 135, 3680-3687 (2013).
- 15. Huang, H., Wong, S. L., Chen, W., Wee, A. T. S., "LT-STM Studies on Substrate-Dependent Self-Assembly of Small Organic Molecules,".J. Phys. D 44, 464005 1-13 (2011).
- 16. Fukuma, T., Kobayashi, K., Yamada, H., Matsushige, K., "Noncontact Atomic Force Microscopy Study of Copper-Phthalocyanines: Submolecular-Scale Contrasts in Topography and Energy Dissipation," J. Appl. Phys. 95, 4742-4746 (2004).

- 17. Wang, C., Liu, X., Wang, C., Xu, X., Li, Y., Xie, F., Gao, Y., "Molecular orientation of copper phthalocyanine thin films on different monolayers of fullerene on SiO2 or highly oriented pyrolytic graphite," Applied Physics Letters 106 (12), (2015).
- 18. Wang, S., Lyu, L., Niu, D., Zhang, L., Huang, H., Gao, Y., "Breaking down and reconstruction of islands during the film growth of CuPc on HOPG," Applied Physics Letters 114 (24), 241602 (2019).
- 19. Yamane, H., Yabuuchi, Y., Fukagawa, H., Kera, S., Okudaira, K. K., Ueno, K., "Does the molecular orientation induce an electric dipole in Cu-phthalocyanine thin films?," J. Appl. Phys. 99, 093705 1-5 (2006).
- 20. Chen, W., Huang, H., Chen, S., Huang, Y. L., Gao, X. Y., Wee, A. T. S., "Molecular orientation-dependent ionization potential of organic thin films," Chem. Mate. 20, 7017-7021 (2008).
- 21. Yamane, H., Kanai, K., Ouchi, Y., Ueno, N., Seki, K., "Impact of interface geometric structure on organic-metal interface energetics and subsequent films electronic structure," Journal of Electron Spectroscopy and Related Phenomena 174 (1-3), 28-34 (2009).
- 22. Masuda, S., Hayashi, H., Harada, Y., "Spatial distribution of the wave functions of a graphite surface studied by use of metastable-atom electron spectroscopy," Phys. Rev. B 42, 3582-3585 (1990).
- 23. Sugiyama, T., Sasaki, T., Kera, S., Ueno, N., Munakata, T., "Intermolecular and interlayer interactions in copper phthalocyanine films as measured with microspot photoemission spectroscopy," Appl. Phys. Lett. 89, 202116 1-3 (2006).
- 24. Petraki, F., Papaefthimiou, V., Kennou, S., "The electronic structure of Ni-phthalocyanine/metal interfaces studied by X-ray and ultraviolet photoelectron spectroscopy," Organic Electronics 8, 522-528 (2007).
- 25. Qian, C., Sun, J., Zhang, L., Huang, H., Yang, J., Gao, Y. L., "Crystal-Domain Orientation and Boundary in Highly Ordered Organic Semiconductor Thin Film," J. Phys. Chem. C 119, 14965–14971 (2015).
- 26. Yang, J. L., Yan, D. H., "Weak Epitaxy Growth of Organic Semiconductor Thin Films " Chem. Soc. Rev. 38, 2634–2645 (2009).
- 27. Palermo, V., Palma, M., Samori, P., "Electronic Characterization of Organic Thin Films by Kelvin Probe Force Microscopy," Adv. Mater. 18, 145–164 (2006).
- 28. de Boer, R. W. I., Stassen, A. F., Craciun, M. F., Mulder, C. L., Molinari, A., Rogge, S., Morpurgo, A. F., "Ambipolar Cu- and Fe-Phthalocyanine Single-Crystal Field-Effect Transistors," Appl. Phys. Lett. 86, 262109 1-3 (2005).
- 29. Shklovskii, B. I., Efros, A. L., [Electronic Properties of Doped Semiconductors], Springer, Berlin, (1984).
- 30. Chwang, A. B., Frisbie, C. D., "Temperature and Gate Voltage Dependent Transport across a Single Organic Semiconductor Grain Boundary," J. Appl. Phys. 90, 1342–1349 (2001).
- 31. Qian, C., Sun, J., Kong, L.-A., Gou, G., Zhu, M., Yuan, Y., Huang, H., Gao, Y. L., Yang, J., "High-Performance Organic Heterojunction Phototransistors Based on Highly Ordered Copper Phthalocyanine/para-Sexiphenyl Thin Films," Adv. Funct. Mater. 2017, 1604933 1-8 (2017).
- 32. Kim, B. J., Ko, Y., Cho, J. H., Cho, J., "Organic Field Effect Transistor Memory Devices Using Discrete Ferritin Nanoparticle Based Gate Dielectrics," Small 9, 3784-3791 (2013).